09

Modified theory of coupled waves and a numerical method for the analysis of Bragg mirrors with an arbitrary refractive index profil

© R.A. Masterov, S.Yu. Karpov

Soft-Impact Ltd,
194044 Saint-Petersburg, Russia
e-mail: roman.masterov@str-soft.com

Received July 7, 2021
Revised July 7, 2021
Accepted August 11, 2021

An analytical and effective numerical approach to the analysis of the optical characteristics of Bragg mirrors with an arbitrary refractive index profile is developed. Analytical expressions obtained using the modified theory of coupled waves for the coefficients of reflection / transmission of light from through the BM with high accuracy predict its main characteristics at both low and high contrast of the refractive index. The hybrid numerical method includes the numerical calculation of the transfer matrix for one period of the knowledge base and its analytical multiplication for an arbitrary number of periods. The developed methods are applied to the analysis of the properties of practically important BMs made on the basis of sprayed pairs of Ta_2O_5/SiO_2 dielectrics, Group III nitrides and arsenides. The characteristics of the knowledge base with smooth (gradient) interfaces are considered in detail.

Keywords: vertically emitting lasers, reflection coefficient, reflection bandwidth.

DOI: 10.21883/TP.2022.15.55270.209-21

Introduction

Because of a high efficiency, low power consumption, high modulation rate, circular shape of the laser bunch, and easily achievable single-mod generation mode and the possibility of integration into a 2D matrix, the vertical cavity surface emitting lasers (VCSELs) have been extensively developed for the last decade. Initially, their application was limited to the data transmission in fiber-optic networks and optical connections in the data processing centers and supercomputers [1]. Next, VCSELs have become popular in the use as directional sources in sensors, laser printers and computer mice [1,2]. Though the demands for VCSELs in the communications market have further constantly grown, these devices have discovered more and more new applications over time. In particular, the needs for safety and social communications on the Internet required creation of fast face recognition systems, where VCSELs were used as compact sources of scanning light [3,4]. Such lasers have also been widely used in compact projectors forming 3*D*-image for cinemas and computer games [5], and the single-mod light generation appeared to be irreplaceable for the creation of atomic clock [6] in positioning and time synchronization systems of various devices and instruments. In biology, the VCSELs are used as the elements of biofluorescent sensors for early stage cancer diagnostics and for drug screening [7]. VCSELs allowed to significantly decrease the size of biofluorescent analysis devices, to make them portable, thus reducing the cost of performed studies. Special advantages of the VCSELs refer to a rapid detection of gaseous ammonia enabling at a high time resolution to assess concentrations of reagents and intermediate products directly in the reaction chamber without sampling and with the possibility of repeated calibration [8]. Finally, the VCSEL matrices are required for the creation of lidars, i.e. systems of detection and determination of distance to the objects by using light [9].

First, the concept of VCSELs creation appeared in 1977 with regard to the AlGaAs/GaAs system of materials providing the laser generation wavelength about 850 nm [1,10]. However, the first experimental embodiment thereof was made in the system of GaInAsP/InP materials with the wavelength of $\lambda = 1300$ nm [11], corresponding to one of the optical fiber transparency windows. Further, the VCSELs studies in these systems of materials have developed in parallel, though a more processable AlGaAs/GaAs system have predominated. The use of InGaAs active area allowed, on the one hand, to decrease the VCSELs threshold currents, on the other hand — to engage the generation wavelength of 980 nm [10]. For the expansion of spectral range of VCSELs to shorter wavelengths ($\lambda = 780$ nm), at first, the same AlGaAs/GaAs system was used [15], and next, the AlGaInP/GaAs system of materials ($\lambda = 670$ nm) [13], whose development was induced by the development of red LEDs. Adoption of blue-purple ($\lambda = 405-450$ nm), and then green ($\lambda = 500-525$ nm) ranges of visible spectrum is caused by the development of group III nitrides, i.e. $AlGaInN/Al_2O_3$ system of materials [14]. Further expansion of operating spectral ranges of VCSELs is associated with a nitride system (in the ultraviolet emission range) [15] and the AlGaInAsSb/GaSb system of materials (in the infrared spectral range) [16].

A crucial element of the VCSELs structure is the Bragg mirrors (BMs) forming a high Q cavity of the laser. The

BMs optimization refers to a complex multifactor task. Its main goal is to obtain the maximum possible laser light reflection factor. Due to possible fluctuations of the thicknesses and refraction indices of the layers constituting BMs, it is necessary to seek for a high reflection index at a minimum number of layers. For this purpose one should select the pairs of materials with high contrast of the refraction index. However, in practice this contrast appears to be considerably different in case of internal BMs made by the alternation of epitaxial semiconductor layers, or external ones formed by the deposition of dielectric films. This is why optimization of the number of pairs of layers, their thicknesses and used materials that determine the refraction index is the first priority task.

However, the use of epitaxial BMs with high contract of the refraction index results in a too high serial resistance of VCSELs due to the generation of high ohmic areas of the spatial charge near to clear heteroboundaries of BMs. In order to decrease the resistance it was suggested to use smooth interfaces and modulated doping of layers of BMs [17–20]. But using the layers with a smooth change of the material composition, as a rule, results in the decrease of the light diffraction efficiency in BMs, consequently, to the fall of its reflectivity, which requires additional optimization of the DM structure. For the purpose it is necessary to use efficient methods of the analysis of optical properties of BMs, operating at random profile of the refraction index.

The use of BMs with smooth interfaces in nitride VCSELs was discussed in [21] in the context of their impact on the BM reflection index. However, in this case the situation is aggravated also by the emergence of polarization charges at the boundaries of the AlGaN/GaN or AlInN/GaN layer pairs, which BMs are usually made of [22]; these charges can significantly change the BMs conductivity both in positive and negative directions depending on the charge sign. Due to this, smooth interfaces are practically applied only at one interface (more frequently, at the upper one [23,24]), by introducing asymmetry into the refraction index distribution. Finally, elastic stresses in BMs caused by the disagreement of lattice constants [25,26] narrow considerably the possibility of selection of pairs of materials with a high contrast of the refraction index, as well as result in the need for the introduction of additional technological layers [26,27] sophisticating the distribution of the refraction index at one period of BMs.

Therefore, the need for the development of efficient and on-the-fly methods of analysis of optical properties of BMs with the random distribution of the refraction index by the period is apparent. The goal hereof refers to the development of an efficient analytical model of BMs, allowing to quickly optimize its structure and obtain distributions of the light intensity inside BMs, as required for the assessment of optical losses, as well as the development of a hybrid numerical approach that combines numerical solution of the Helmholtz equation in one BM period, by using the matrix method allowing to analyze the properties of the entire multiperiod BM. These approaches are used hereinafter for the analysis of BMs with different refraction index profiles.

1. Theory

Let us consider BM referring to a medium with periodically varying permittivity $\varepsilon(z+a) = \varepsilon_r(z) + i\varepsilon_i(z)$, that generally includes a real ε_r and imaginary ε_i parts, where a is the period of the structure (Fig. 1). Usually, $\varepsilon_r(z) \gg \varepsilon_i(z)$, then the imaginary part $\varepsilon_i(z) = \alpha(z)\varepsilon_r^{1/2}(z)/k$ is expressed in terms of the light absorption constant α, and the real part $\varepsilon_r(z) = n^2(z)$ — in terms of the refraction index n. BM is located between media with the refraction indices n_i and n_t. The incident wave with the amplitude of A_i comes to BM from the left from the medium with the refraction index of n_i, and the reflected wave with the amplitude A_r leaves to the same medium. The wave transmitted through BM with the amplitude of A_t goes to the medium with the refraction index of n_t (Fig. 1).

In the $1D$-approximation the electromagnetic wave is described by the Helmholtz equation relative to the amplitude of the electrical field $E(z,t)$:

$$\frac{d^2E(z)}{dz^2} + k^2\varepsilon(z)E(z) = 0, \quad E(z,t) = E(z)\exp(-i\omega t), \tag{1}$$

where z is the coordinate oriented by normal to the BM layers, $k = 2\pi/\lambda$ is the wave vector, λ is the light wavelength in the vacuum. Magnetic field of the light wave is expressed in terms of the electrical field as $H(z) = (i/k)dE(z)/dz$.

The continuity of electrical and magnetic field refers to limiting conditions on the external and internal BM interfaces, which means the continuity E and the derivative dE/dz.

1.1. Modified Coupled-Wave Theory

Initially, the coupled-wave theory was proposed by Kogelnik and Shank [28] for the analysis of periodic dielectric structures. It is applicable, if the amplitude

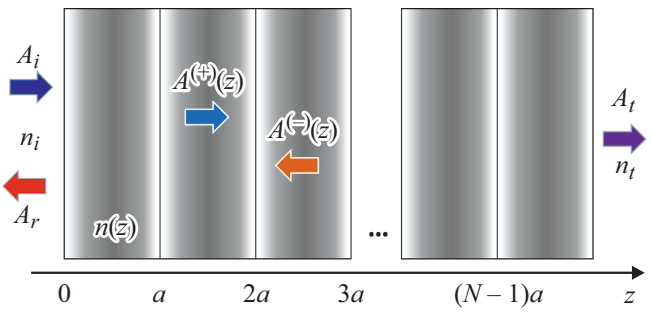

Figure 1. The schematic structure of the Bragg mirror, the amplitude of direct $A^{(+)}(z)$ and inverse $A^{(-)}(z)$ waves in the structure, as well as the amplitude of incident A_i, reflected A_r and transmitted A_t waves.

of permittivity modulation $\Delta\varepsilon$ is low versus its average value ε_0: $\Delta\varepsilon/\varepsilon_0 \ll (\pi m)^{-1}$, where m is the diffraction order, which BM is configured to [29]. Therefore, it can also be seen that the applicability of the Kogelnik and Shank approach is not also limited to low diffraction orders.

However, in case of the most frequently used BMs of the alternating pairs of layers with high contrast of the refraction index, the prediction error in this theory becomes quite high. The work [30] proposed a modified coupled-wave theory (MCWT) with considerably more extensive applicability, where the multiwave light diffraction is partially considered, especially in case of high diffraction orders, by changing the expressions for the coupling coefficients. Consideration of the multiwave diffraction allows to expand the MCWT applicability, which formally can be expressed as $\Delta\varepsilon/\varepsilon_0 \ll (\pi m)^{-1} + \pi m$ [29]. Moreover, MCWT is working well both in the case of continuously varying permittivity, and in the case of discrete one. Therefore, it is the MCWT that appears to be the optimum one for the development of an analytical theory of light propagation in BMs.

According to [30], the solution of equation (1) is to be found by the formula

$$E(z) = \frac{1}{\varepsilon^{1/4}(z)} \Big\{ A^{(+)}(z) \exp[i\psi(z)] + A^{(-)}(z) \exp[-i\psi(z)] \Big\}, \tag{2}$$

where the phase

$$\psi(z) = k \int_0^z \varepsilon^{1/2}(z')dz' \cong k \int_0^z n(z')dz' + \frac{1}{2} i \int_0^z \alpha(z')dz', \tag{3}$$

and $A^{(+)}(z)$ and $A^{(-)}(z)$ are slowly changing amplitudes of the direct and inverse waves in BM. Solution of the main equations of MCWT [30] provides the following general expressions for these amplitudes:

$$A^{(+)}(z) = C_1 \exp(-\gamma_- z) + C_2 \exp(\gamma_+ z),$$

$$A^{(-)}(z) = C_1 r_B^{\infty} \exp(-\gamma_+ z) - \frac{\kappa_{-n}^{(+)}}{\kappa_n^{(-)} r_B^{\infty}} C_2 \exp(\gamma_- z). \tag{4}$$

Here $\gamma_\pm = \gamma \pm \left(\frac{1}{2}\alpha_0 - i\delta\right)$, $\gamma = \left[\left(\frac{1}{2}\alpha_0 - \delta\right)^2 + \right.$ $\left. + \kappa_{-m}^{(+)} \kappa_m^{(-)}\right]^{1/2}$ is the complex wave number, such that $\mathrm{Re}\,\gamma \geq 0$, $n_0 = a^{-1} \int_0^a n(z)dz$ and $\alpha_0 = a^{-1} \int_0^a \alpha(z)dz$ — averaged by period refraction index and optical losses coefficient, $\delta = kn_0 - -(\pi/a)m$ — offset from the Bragg resonance of the m-th order, C_1 and C_2 are arbitrary constants, and the parameter $r_B^{\infty} = -\kappa_{-m}^{(+)}/(\gamma + \frac{1}{2}\alpha_0 - i\delta)$ refers to the amplitude light refraction index from semi-infinite BM [29].

The coupling coefficients $\kappa_m^{(\pm)}$ of direct and inverse waves corresponding to the m-th order of diffraction are determined in MCWT by expressions

$$\kappa_m^{(\pm)} = \frac{1}{a} \left\{ \int_0^a \frac{dz}{4\varepsilon} \frac{d\varepsilon}{dz} \exp\left[2i \left(\pm\psi(z) m \left(kn_0 + \frac{1}{2} i\alpha_0 \right) z - \frac{\pi}{a} mz \right) \right] + \frac{1}{4} \sum_{j=1}^{p} \ln \frac{\varepsilon(z_j + 0)}{\varepsilon(z_j - 0)} \exp\left[2i \times \left(\pm\psi(z_j) m \left(kn_0 + \frac{1}{2} i\alpha_0 \right) z_j - \frac{\pi}{a} mz_j \right) \right] \right\}, \tag{5}$$

where the integral is understood as the main value, the second element refers to the apparently figured out contribution from interfaces with discrete permittivity, and z_j $(j = 1, 2 \ldots p)$ are the coordinates of these interfaces.

The limit conditions for the Helmholtz equation at $z = 0$ and L, assuming the continuity of tangential components of electrical and magnetic fields provide four ratios, which at the specified amplitude A_i allow to determine the constants C_1 and C_2, the amplitudes of transmitted (A_t) and reflected (A_r) waves, as well as the amplitude reflection indices

$$r_\Sigma^L = \frac{r_i + \tilde{r}}{1 + r_i \tilde{r}}, \quad \tilde{r} = \frac{r_B^L + Y_B r_t \exp(2i\varphi_t)}{1 + r_B^L (\kappa_m^{(-)}/\kappa_m^{(+)}) r_t \exp(2i\varphi_t)},$$

$$r_i = \frac{n_i - \varepsilon_r^{1/2}(0)}{n_i + \varepsilon_r^{1/2}(0)}, \quad r_t = \frac{\varepsilon_r^{1/2}(L) - n_t}{\varepsilon_r^{1/2}(L) + n_t},$$

$$r_B^L = \frac{-\kappa_{-m}^{(+)} \mathrm{sh}(\gamma L)}{\gamma\, \mathrm{ch}(\gamma L) + \left(\frac{1}{2}\alpha_0 - i\delta\right) \mathrm{sh}(\gamma L)},$$

$$Y_B = \frac{\gamma\, \mathrm{ch}(\gamma L) - \left(\frac{1}{2}\alpha_0 - i\delta\right) \mathrm{sh}(\gamma L)}{\gamma\, \mathrm{ch}(\gamma L) + \left(\frac{1}{2}\alpha_0 - i\delta\right) \mathrm{sh}(\gamma L)} \tag{6a}$$

and the transmissivity

$$t_\Sigma^L = \frac{(1 + r_i)(1 + r_t)}{1 + r_i \tilde{r}} \cdot \frac{t_B^L}{1 + r_B^L (\kappa_m^{(-)}/\kappa_{-m}^{(+)}) r_t \exp(2i\varphi_t)},$$

$$t_B^L = \frac{\varepsilon^{1/4}(0)}{\varepsilon^{1/4}(L)} \cdot \frac{\gamma \exp(i\varphi_t)}{\gamma\, \mathrm{ch}(\gamma L) + \left(\frac{1}{2}\alpha_0 - i\delta\right) \mathrm{sh}(\gamma L)} \tag{6b}$$

of light through BM. Then, energetic reflection index (R_B^L) and the transmissivity (T_B^L) from/through BM are

$$R_B^L = |r_\Sigma^L|^2 \quad \text{and} \quad T_B^L = (n_t/n_i)|t_\Sigma^L|^2. \tag{7}$$

In the absence of light absorption, the ratio $R_B^L + T_B^L = 1$ is observed in the Bragg mirror. Distribution of the light intensity in the Bragg mirror is specified by the direct calculation of $|E(z)|^2$ with the use of expression (2).

1.2. Numerical method of calculation

For the calculation of the characteristics of BM made of alternating pairs of layers with constant permittivity inside each layer, usually, the efficient transfer matrix method is used [31]. According to this method, amplitudes of direct and inverse wave at a random point $z = z_0$ are associated with the amplitudes of these waves at the point $z = z_0 + a$ by matrix ratio

$$\begin{bmatrix} A^{(+)(z_0)} \\ A^{(-)(z_0)} \end{bmatrix} = \begin{bmatrix} m_{11} & m_{15} \\ m_{21} & m_{22} \end{bmatrix} \cdot \begin{bmatrix} A^{(+)(z_0+a)} \\ A^{(-)(z_0+a)} \end{bmatrix}, \qquad (8)$$

where m_{ik} $(i, k = 1, 2)$ are complex elements of the transfer matrix having analytical form in case of the layer pairs with constant permittivity [31]. Since transfer matrices are unimodular, we can obtain directly the coupling of amplitudes of direct and inverse waves at opposite ends of BM containing N pairs of layers:

$$\begin{bmatrix} A^{(+)(0)} \\ A^{(-)(0)} \end{bmatrix} = \begin{bmatrix} M_{11} & M_{15} \\ M_{21} & M_{22} \end{bmatrix} \cdot \begin{bmatrix} A^{(+)(L)} \\ A^{(-)(L)} \end{bmatrix}, \ \beta = \frac{1}{2}(m_{11} + m_{22}),$$
$$M_{11} = m_{11}\mathscr{U}_{N-1}(\beta) - \mathscr{U}_{N-2}(\beta), \quad M_{15} = m_{15}\mathscr{U}_{N-1}(\beta),$$
$$M_{21} = m_{21}\mathscr{U}_{N-1}(\beta) \quad M_{22} = m_{22}\mathscr{U}_{N-1}(\beta) - \mathscr{U}_{N-2}(\beta), \qquad (9)$$

where $\mathscr{U}_N(\beta)$ is the 2-th kind Chebyshev polynomial, for the calculation of which there are well-known recurrent ratios.

In case of BMs with a complex permittivity profile the transfer matrix elements cannot be obtained analytically. In order to generally preserve the matrix method advantages in case of random distribution of permittivity in the BM period, the Helmholtz equation was numerically solved in one period, the matrix elements m_{ik} were retrieved from that solution, and then ratio (9) was used to obtain the coupling of amplitudes of direct and inverse waves at different ends of BM.

With the known elements M_{ik} of the full transfer matrix, from the limit conditions, one can derive amplitude reflection indices

$$r_\Sigma^L = \frac{r_i + \tilde{r}}{1 + r_i\tilde{r}}; \quad \tilde{r} = \frac{M_{21} + M_{22}r_t}{M_{11} + M_{15}r_t} \qquad (10a)$$

and transmissivity

$$t_\Sigma^L = \frac{(1 + r_i)(1 + r_t)}{(1 + r_i\tilde{r})(M_{11} + M_{15}r_t)} \qquad (10b)$$

of light from/through BM. Here r_i and r_t are the amplitude Fresnel reflection indices of light from the first and last interfaces of BM, accordingly. Energetic reflection indices are still calculated by using formulae (7).

2. Results

2.1. Bragg mirror with constant refraction indices of layers

The BMs of typical VCSELs structures based on group III nitrides were taken as an example of calculation [32,33]. One of such BMs was made of 50 pairs of $Al_{0.18}In_{0.82}N/GaN$ layers configured to the light wavelength $\lambda_0 = 410$ nm, with the last GaN-layer. Another BM included 35 pairs of layers $Al_{0.15}In_{0.85}N/Al_{0.2}Ga_{0.8}N$ configured to the wavelength $\lambda_0 = 343$ nm, with the last $Al_{0.2}Ga_{0.8}N$-layer. These BMs forming a part of epitaxial structures of lasers and usually grown in thick GaN-layers must ensure the maximum full reflection of the generated light. For comparison with the results of characterization of such BMs presented in [32,33], it was assumed that the light falling onto them comes from the air. A typical structure of the Ta_2O_5/SiO_2 layer pairs configured to the wavelength of 410 nm, with the last SiO_2-layer was taken as another example of BM emitting the light from the laser. It was assumed that such a multilayered structure is applied by the deposition of Ta_2O_5 and SiO_2 onto GaN, and the light, once having passed through it, goes into the air. The refraction indices of materials used in BMs given in Table were taken from [34,35] (in case of group III nitrides, the refraction indices of ordinary waves were used as such). In order to obtain the maximum light reflection index at the minimum number of BM layers, their thicknesses d_1 and d_2 were selected equal to a quarter of the light wavelength in a substance, i.e. $d_{1,2} = \frac{1}{4}\lambda_0/n_{1,2}$, where n_1 and n_2 are refraction indices of the BM layer pairs [31].

Fig. 2 shows spectral dependences of the energetic reflection index Ta_2O_5/SiO_2 of BM with 15 layer pairs obtained by means of MCWT (black line) and by the transfer matrix method [31] (grey line) providing therein the accurate task solution. In calculations we ignored dispersion of the refraction indices of both dielectrics. It can be seen that within the BM reflection band both methods with graphical accuracy provide virtually the same results, regardless of a high contrast of the refraction indices Ta_2O_5 and SiO_2. The half-height reflection band width the same is well predicted: $\Delta R = 131$ nm. At that the error of prediction of the first maxima of the reflection index beyond the limits of that band does not exceed 10%.

The behavior of the MCWT prediction errors is better understood by analyzing the dependence of the maximum value of the BM reflection index (at the wavelength of 410 nm) on the number of the Ta_2O_5 and SiO_2 layer pairs (Fig. 2, *b*). Since MCWT has been specially developed for periodic structures, it was expected that his will be poorly applicable to a low number of pairs. However, it appears that even for two pairs of layers the error of the reflection index determination by MCWT becomes $\sim 10\%$, and for five pairs it falls to $\sim 1\%$, with further exponential decrease along with the number of layer pairs. Therefore, MCWT can be used for the prediction of the BM reflection index value and the reflection band width with a quite good accuracy.

In terms of the characteristics of the Ta_2O_5/SiO_2 BMs, Fig. 2, *b* shows that the maximum reflection index is virtually achieved even with 10 pairs of layers of Ta_2O_5 and SiO_2. It is interesting that calculations show an increase of that number of layers up to 15–16 in case of the light falling onto BMs from the air. It is the number of layers Ta_2O_5 and SiO_2, which is used in practice [36,37].

Characteristics of Bragg mirror materials. Media, from which the light falls onto the mirror and the media, into which the light is emitted

Bragg mirror	Material	Index of refraction	Indices of refraction n_i/n_t
$50\cdot(Al_{0.18}In_{0.82}N/GaN)$	GaN	2.53	1.0/2.53
	$Al_{0.18}In_{0.82}N$	2.28	
$35\cdot(Al_{0.15}In_{0.85}N/Al_{0.2}Ga_{0.8}N)$	$Al_{0.2}Ga_{0.8}N$	2.61	1.0/2.71
	$Al_{0.15}In_{0.85}N$	2.345	
$15\cdot(Ta_2O_5/SiO_2)$	SiO_2	1.47	2.53/1.0

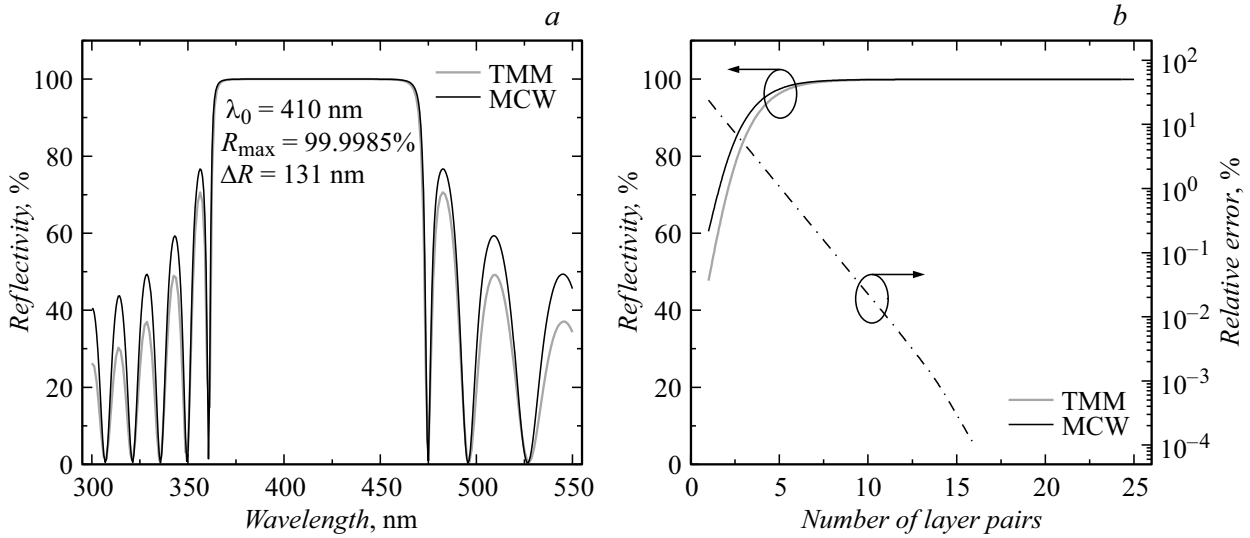

Figure 2. The spectral dependence of the energetic reflection index of the Ta_2O_5/SiO_2 BM (a) and the dependence of the reflection index at the wavelength of 410 nm on the number of layer pairs (b). The black solid line refers to calculations under the modified coupled-wave theory (MCW), and the grey one refers to accurate results obtained by the transfer matrix method (TMM); the dash-dot line shows the relative error of calculation of the coupled-wave theory.

Fig. 3 shows spectral dependences of energetic reflection indices of the $Al_{0.18}In_{0.82}N/GaN$ (a) and $Al_{0.15}In_{0.85}N/Al_{0.2}Ga_{0.8}N$ BMs calculated by means of MCWT (black line) and by means of the TMM (grey line). Comparison of the calculation results between these two methods shows a low difference between the values of the reflection index within a wide spectral range. It is associated with a relatively low contrast of the refraction indices of the semiconductors forming part of BM. The maximum values of the reflection indices were 99.9949% and 99.9123%, and half-widths of the reflection bands — 30.1 and 27.3 nm for the $Al_{0.18}In_{0.82}N/GaN$ and $Al_{0.15}In_{0.85}N/Al_{0.2}Ga_{0.8}N$ BMs, accordingly. The following reflection indices and half-widths of the reflection bands were experimentally obtained on these BMs grown by the MOC-hydride epitaxy: 99.7% and 30 nm for the 410 nm wavelength and 99.5% and 20 nm for the 343 nm wavelength. As we can see from the comparison with theoretical predictions, a considerable disagreement is observed only for the half-width of the reflection band of the $Al_{0.15}In_{0.85}N/Al_{0.2}Ga_{0.8}N$ BMs. In our opinion, this can be related to fluctuations of the layer thicknesses of that BM, occurring in the process of growing thereof. Another possible reason refers to elastic stresses occurring in the structure during its growing on the GaN-buffer layer that results in bending of epitaxial structure, in general.

The light intensity distribution inside BMs often appears demanded during the analysis of VCSELs. Such distributions corresponding to the light wavelength of 410 nm are shown in Fig. 4 for the Ta_2O_5/SiO_2 and $Al_{0.18}In_{0.82}N/GaN$ Bragg mirrors. It can be seen that the distribution of intensity obtained by means of MCWT is subjected to non-physical disruptions associated with direct inclusion into the amplitudes of permittivity $\varepsilon^{-1/4}(z)$ (see expression (2)), which is discrete itself in the cases found by us. A reverse side of that disadvantage is a quite accurate reproduction of the light intensity profile far from disruptions. Moreover, in case of decrease of the refraction index contrast in BMs, availability of disruptions becomes low significant (Fig. 4, b).

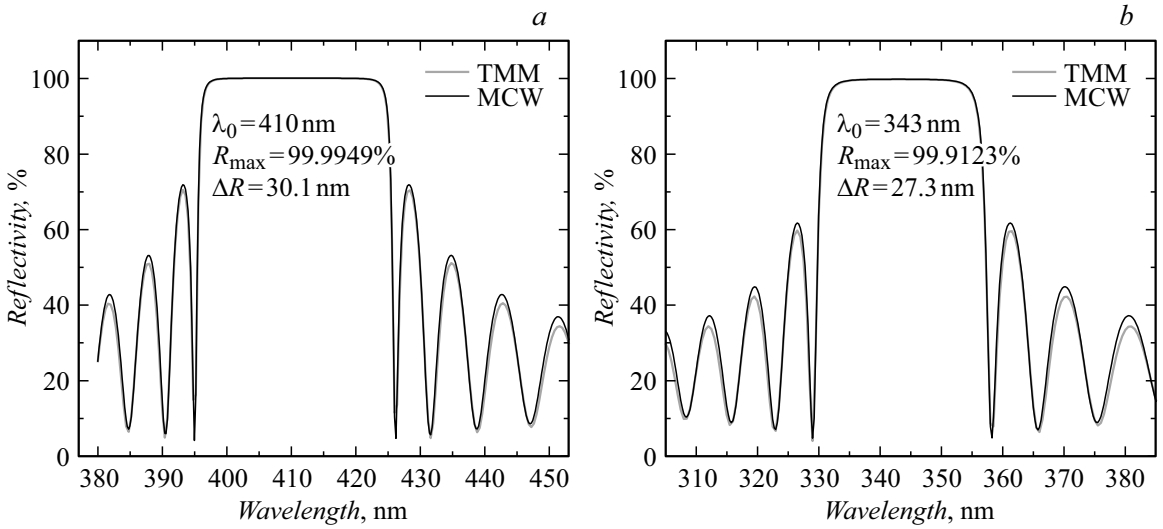

Figure 3. Spectral dependences of the energetic reflection indices of $Al_{0.18}In_{0.82}N/GaN$ (*a*) and $Al_{0.15}In_{0.85}N/Al_{0.2}Ga_{0.8}N$ (*b*) BMs. The black solid line refers to calculations under the modified coupled-wave theory (MCW), and the grey one refers to accurate results obtained by the transfer matrix method (TMM).

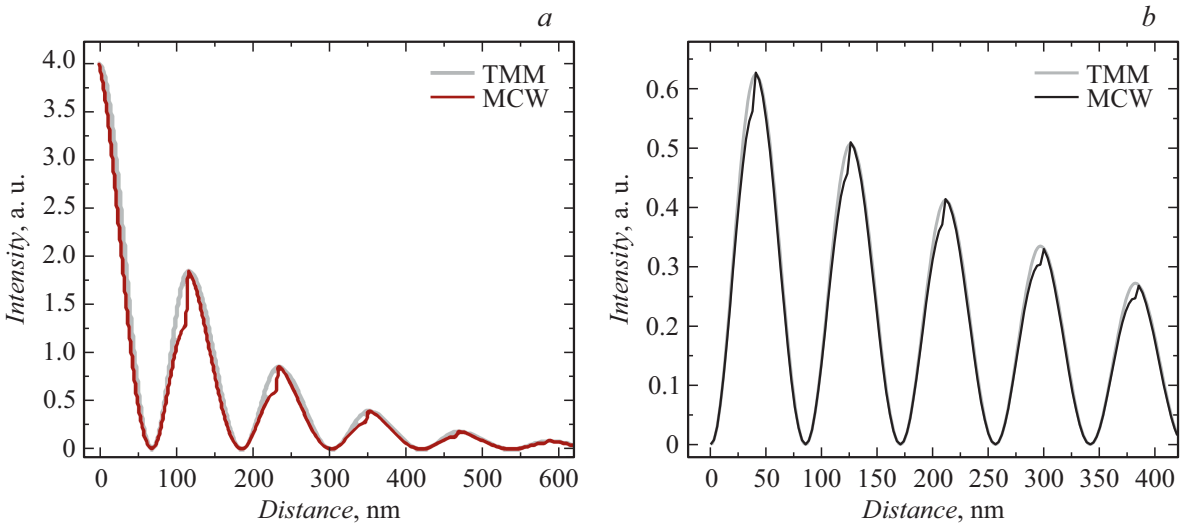

Figure 4. Distributions of the light intensity inside Ta_2O_5/SiO_2 (*a*) and $Al_{0.18}In_{0.82}N/GaN$ (*b*) of the Bragg mirrors at the wavelength of 410 nm. The black solid line refers to calculations under the modified coupled-wave theory (MCW), and the grey one refers to accurate results obtained by the transfer matrix method (TMM).

2.2. Optical properties of BMs with gradient interfaces

In order to reduce electrical resistance of BMs made on the basis of triple semiconductor solid solutions, the composition profiles are usually used with a smooth (gradient) transition from a wide-zone material having lower refraction index to a narrow-zone material having higher refraction index [17–20]. In this case, the assessment of optical characteristics of BMs and optimization of their structure, including the number of periods required for the implementation of a high reflection index becomes a non-trivial task. In this section, MCWT is used for the solution of this task. Due to the absence of accurate solution of the Maxwell equations for a random profile of the refraction index, the results obtained by means of MCWT are compared with numerical calculations performed by the method described in sect. 2.2.

Not all solid solutions allow to produce BMs with a random composition profile by using epitaxy. First of all it relates to the generation of elastic stresses in epitaxial structures due to the disagreement of the crystalline lattice constants of binary components of solid solutions. There is no such problem in AlGaAs solid solutions which are agreed in terms of the lattice constant with GaAs within the whole composition change range. For that reason, we selected BMs with triangular and ragged profiles of the

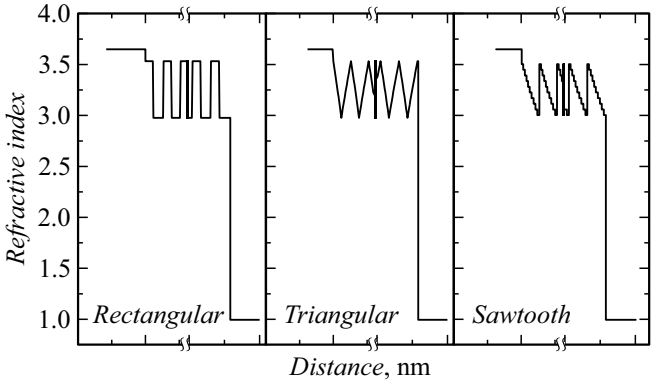

Figure 5. Profiles of the refraction index in the Bragg mirrors, analyzed herein.

refraction index as practically relevant examples (Fig. 5). At that, the minimum and maximum values of the refraction index were selected as corresponding to solid solutions of $Al_{0.92}Ga_{0.08}As$ and $Al_{0.16}Ga_{0.84}As$.

Each BM was considered as consisting of 25 periods. It was assumed that the light comes to BM from the GaAs layer, and released into the air. Resulting profiles of the refraction index of the task in general are given in Fig. 5. A rectangular profile of the refraction index is shown there for comparison, where one period includes the quarter wave (for the wavelength $\lambda_0 = 850\,\text{nm}$) layers of $Al_{0.92}Ga_{0.08}As$ and $Al_{0.16}Ga_{0.84}As$ with the thickness of 71.36 and 60.15 nm, accordingly. The periods of all three BMs were selected similar.

Fig. 6, *a, b* shows spectral dependences of the BMs reflection indices with triangular and ragged profile of the refraction index, accordingly, obtained by using MCWT (black lines) and numerical method (grey lines). It can be seen that the maxima of the reflection indices in both methods are considerably shifted towards the long wavelength side relative the light wavelength $\lambda_0 = 850\,\text{nm}$, which BM with the rectangular refraction index is configured to. The shift is different for MCWT and the numerical method; it is because MCWT operates with the quasiclassical phase of the propagating wave $\psi(z)$ (see expression (3)), and the numerical method finds the phase directly from the Helmholtz equation. The presence of red shift predicted by both methods indicates that accurate configuration of BM to the required wavelength cannot be based on the estimates developed for the rectangular refraction index, but needs detailed calculations and corrections of the BM period, which are based on them.

The maximum values of the BM refraction indices both with triangular and ragged profile appear to be lower than for BM with a rectangular profile of the refraction index. It is especially clear in Fig. 6, *c* and *d* showing the dependences of the reflection indices at the wavelength of $\lambda_0 = 850\,\text{nm}$ on the number of BM periods. As we can see, in the case of a rectangular profile the reflection index is saturated yet at 15 periods, meanwhile 25 and more periods are required for triangular and ragged profiles. It means that reduction of the BM resistance by using smooth interfaces requires thorough optimization of the number of its periods. The reason for the refraction index impact on the reflection index is easily interpreted in terms of the coupling constant introduced in MCWT. Truly, the absolute value of the coupling constant $|\kappa_m^{(\pm)}|$ for the rectangular profile of the refraction index ($12996\,\text{cm}^{-1}$) appears to be several times higher than that of the ragged profile ($6412\,\text{cm}^{-1}$) or the triangular ($8181\,\text{cm}^{-1}$) one. Since it is the coupling constant that finally determines both the maximum reflection index and the reflection band width, the impact of the refraction index profile on that constant appears to be determinant for the optical characteristics of BMs.

An interesting feature of the spectral dependence of the reflection index shown in Fig. 6, *a* is the asymmetry of its shoulders relative to the wavelength, corresponding to the reflection maximum, and a considerable level of reflection on the right from the main spectral band. The specially performed modeling has shown that these features are mainly determined by the Fresnel reflection of light at the BM output interface. In fact, in case of 25 periods and the triangular profile of the refraction index of BMs, the reflection index has only started saturating, so the light reflection at the BM output interface appears to be significant. When the refraction indices are agreed at this interface (not shown here) the values of reflection coefficient beyond the main spectral band decrease, and the nature of asymmetry changes, however, not disappears completely. In our opinion the latter can be associated with the residual contribution of the Fresnel reflection at the input interface into the total light reflection from BMs.

By comparing the results obtained by means of MCWT and numerical method, it should be noted that, except for the spectral shift of the BM reflection band, both methods provide quite similar results both for the maximum value of the reflection index, and for the width of that band. It occurs both in case of continuously varying refraction index (triangular profile), and in case of discrete-continuous change (ragged profile). The dependences of the reflection index on the number of BM periods appear to be similar as well (see Fig. 6, *c* and *d*). The absence of disruptions of permittivity in the triangular profile allows to eliminate non-physical disruptions in the intensity distribution in BMs similar to those described in sect. 2.1, however, a small deviation of the intensity values occurs near to its maxima, as predicted by means of MCWT with regard to those obtained numerically (not shown herein). In general this deviation is lower than that for discrete profiles of permittivity, therefore it has a low relevance.

Conclusion

The work is aimed at the development of efficient methods of the analysis of optical characteristics of BMs with the random profile of the refraction index, which is important

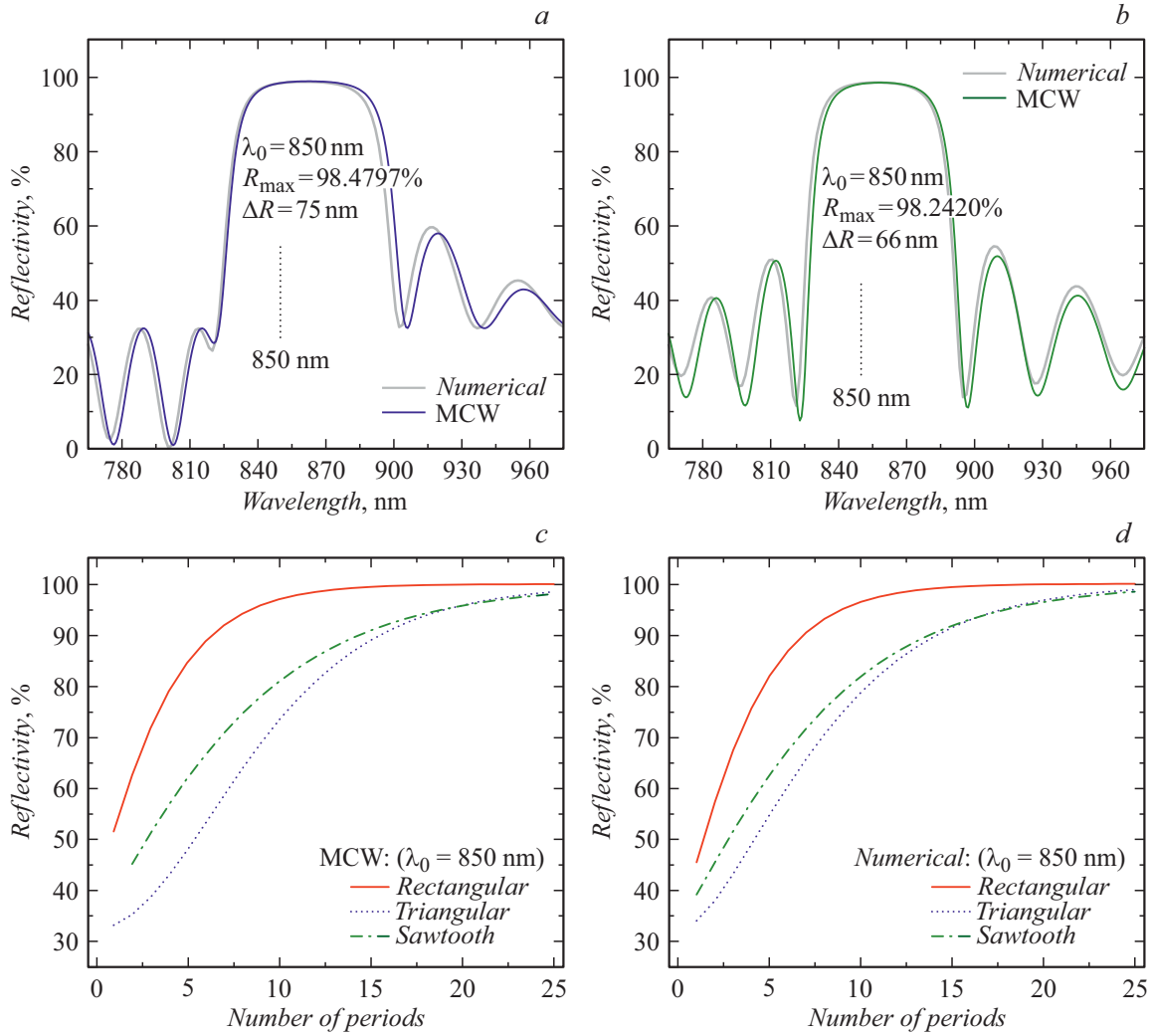

Figure 6. Spectral dependences of energetic reflection indices on the $Al_{0.92}Ga_{0.08}As/Al_{0.16}Ga_{0.84}As$ BMs with triangular (*a*) and ragged (*b*) profile of the refraction index and 25 periods. Dependence of the reflection index of such BMs at the light wavelength of 850 nm on the number of periods obtained by means of MCWT (*c*) and the numerical method (*d*); here the results for rectangular refraction profile are also included for comparison.

for the practical optimization of its electrical parameters. Based on MCWT taking the multiwave light diffraction into account, we obtained analytical expressions for the light reflection/transmissivity indices from/through BMs with the random profile of the refraction index. A hybrid algorithm of numerical calculation of these indices was developed as an alternative approach. The algorithm is based on the numerical construction of the transfer matrix within one period of BM with further analytical multiplication thereof for the obtainment of optical characteristics of the mirror with a random number of periods. Such an approach enables to avoid the error accumulation in direct numerical calculation of the whole BM and considerably accelerates the obtainment of the final outcome.

Based on the BM example with the rectangular profile of the refraction index that assumes an accurate solution, it is shown that MCWT predicts at high accuracy such important BM characteristics as the maximum value of the light reflection index and its spectral dependence, including the half-height reflection band width. The same conclusion is also confirmed for BMs with smooth (gradient) interfaces by comparing the results obtained by means of MCWT, and the numerical hybrid approach.

The standard coupled-wave theory [28] is well applicable in case of a low contrast of the refraction index in BM. By comparing the results with accurate solution assumed for the rectangular profile of the refraction index it is shown that MCWT at high accuracy predicts optical characteristics of BMs both in case of low, and high contrast of the refraction index, which is associated with a thorougher consideration of the multiwave diffraction under this method [29,30].

The following can be noted as disadvantages of MCWT:

1) non-physical disruptions in distribution of the light intensity inside of BMs occurring due to the introduction of the discrete distribution of permittivity into the expression for intensity (2).

2) shift of spectral dependence of the BM reflection index with smooth interfaces obtained by means of MCWT relative to the numerically calculated one. The shift occurs due to the use of a quasiclassical phase of the propagating wave, meanwhile the phase in the numerical method is derived directly from the Helmholtz equation. However, its value is low — it is only 1 to 3% of the reflection band width, which is not critical for the practical calculations.

Subject to the above mentioned conclusions one can recommend the use of MCWT, first of all, for the analysis of the maximum value of the light reflection index from BMs and the reflection band width.

Comparison of the results of our calculations with experimental data on the light reflection from $Al_{0.18}In_{0.82}N/GaN$ and $Al_{0.15}In_{0.85}N/Al_{0.2}Ga_{0.8}N$ of BMs has shown in general their good agreement with each other. An exclusion is considerably lower experimental reflection band width of $Al_{0.15}In_{0.85}N/Al_{0.2}Ga_{0.8}N$ of BMs, which is associated, in our opinion, either with fluctuations of the thicknesses and compounds of epitaxial layers, or with elastic stresses in BM resulting in bending of the epitaxial structure as a whole.

By means of modeling it is shown that configuration of the maximum reflection index of BMs to the desired light wavelength is a non-trivial task for the random distributions of the refraction index in the period, including those with smooth interfaces. This configuration requires preliminary calculation of the spectral dependence of the reflection index and based on its outcome — correction of the BM period. Due to the practical relevance of that task, an accurate configuration could require several iterations.

By means of modeling it was found that transition from the stepped profile to profiles with smooth (gradient) interfaces, necessary for the BM resistance decrease, is accompanied by the reduction of the maximum reflection index and narrowing of the reflection band. However, these negative trends can be compensated by the increase of the number of periods in BMs.

It shown that in case of insufficient number of periods in BMs, the Fresnel reflection of light at the output interface could considerably impact the spectral dependence of the reflection index. Manifestations of such impact could be, in particular, first, a high asymmetry of spectral dependence of the reflection index relative to the configuration wavelength λ_0, and, second, a high level of the light reflection beyond the limits of the main spectral band. The last effect, basically, could result in the emergence of parasitic generation in VCSELs beyond the limits of the reflection band of BMs. In case of increase of the number of periods of BMs such impact of the Fresnel reflection is attenuated.

Conflict of interest

The authors declare that they have no conflict of interest.

References

[1] K. Iga. Japanese J. Appl. Phys., **57** (8S2), 08PA01 (2018). DOI: 10.7567/JJAP.57.08PA01

[2] K.J. Ebeling, R. Michalzik. *VCSEL Technology for Imaging and Sensor Systems Applications.* In: 22nd Microoptics Conf. IEEE, (2017), p. 20–21. DOI: 10.23919/MOC.2017.8244477

[3] E. Watanabe, K. Kodate. *Multi-Light Source Compact Optical Parallel Correlator (MLCOPaC) for Facial Recognition Using VCSEL Array.* In: 19th Congress of the International Commission for Optics: Optics for the Quality of Life International Society for Optics and Photonics, (2003), p. 208–209. DOI: 10.1117/12.523842

[4] E. Watanabe, N. Takeda, K. Kodate. *Fabrication and Evaluation of a Facial Recognition System Based on PJTC Using Two-Dimensional VCSEL Array Module.* In: Practical Holography XVII and Holographic Materials IX International Society for Optics and Photonics, (2003), v. 5005, p. 345–356. DOI: 10.1117/12.473886

[5] S. McEldowney. U.S. Patent N 8,320,621. Washington, DC: U.S. Patent and Trademark Office (2012).

[6] D.K. Serkland, G.M. Peake, K.M. Geib, R.Lutwak, R.M. Garvey, M. Varghese, M. Mescher. *VCSELs for Atomic Clocks.* In Vertical-Cavity Surface-Emitting Lasers X. International Society for Optics and Photonics, (2006), v. 6132, p. 613208. DOI: 10.1117/12.647095

[7] E. Thrush, O. Levi, W. Ha, G. Carey, L.J. Cook, J. Deich, S.J. Smith, W.E. Moerner, J.S. Harris. IEEE J. Quant. Electron., **40** (5), 491 (2004). DOI: 10.1109/JQE.2004.826440

[8] G. Totschnig, M. Lackner, R. Shau, M. Ortsiefer, J. Rosskopf, M.C Amann, F. Winter. Appl. Phys. B, **76** (5), 603 (2003). DOI: 10.1007/s00340-003-1102-1

[9] A. Lipson. U.S. Patent N 9,831,630. Washington, DC: U.S. Patent and Trademark Office (2017).

[10] K. Iga. *Vertical-Cavity Surface-Emitting Laser: Introduction and Review.* In *Vertical-Cavity Surface-Emitting Laser Devices* (Springer, Berlin, Heidelberg, 2003), DOI: 10.1007/978-3-662-05263-1_1

[11] H. Soda, K.I. Iga, C. Kitahara, Y. Suematsu. Jpn. J. Appl. Phys., **18** (12), 2329 (1979). DOI: 10.1143/JJAP.18.2329

[15] M.H. Crawford. OSA Trends in Optics and Photonics Series, **15**, 104 (1998).

[13] T. Sakaguchi, T. Shirasawa, N. Mochida, A. Inoue, M. Iwata, T. Honda, F. Koyama, K. Iga. *Highly reflective AlN–GaN and ZrO/sub 2/–SiO/sub 2/multilayer Reflectors and Their Applications for InGaN–GaN Surface Emitting Laser Structures.* In Conf. Proceedings. LEOS'98. 11th Annual Meeting. IEEE Lasers and Electro-Optics Society 1998 Annual Meeting. IEEE, (1998), v. 1, p. 34–35. DOI: 10.1109/LEOS.1998.737719

[14] D. Kasahara, D. Morita, T. Kosugi, K. Nakagawa, J. Kawamata, Y. Higuchi, H. Matsumura, T. Mukai. Appl. Phys. Express, **4** (7), 072103 (2011). DOI: 072103.10.1143/APEX.4.072103

[15] A.V. Nurmikko, J. Han. *Progress in Blue and Near-Ultraviolet Vertical-Cavity Emitters: A status report. In: Vertical-Cavity Surface-Emitting Laser Devices.* (Springer, Berlin, Heidelberg, 2003), p. 343. DOI: 10.1007/978-3-662-05263-1_11

[16] S. Arafin, H. Jung. *Recent Progress on GaSb-Based Electrically-Pumped VCSELs for Wavelengths Above 4 μm.* In *Image Sensing Technologies: Materials, Devices, Systems, and Applications VI*, (2019), v. 10980, p. 109800H. DOI: 10.1117/12.2522418
[17] E.F. Schubert, L.W. Tu, G.J. Zydzik, R.F. Kopf, A. Benvenuti, M.R. Pinto. Appl. Phys. Let., **60** (4), 466 (1992). DOI: 10.1063/1.106636
[18] M.G. Peters, B.J. Thibeault, D.B. Young, J.W. Scott, F.H. Peters, A.C. Gossard, L.A. Coldren. Appl. Phys. Lett., **63** (25), 3411 (1993). DOI: 10.1063/1.110156
[19] A. Mutig. *Physical Processes in Lasers and VCSEL Design.* In: *High Speed VCSELs for Optical Interconnects* (Springer, Berlin, Heidelberg, 2011)
[20] S.A. Chalmers, K.L. Lear, K.P. Killeen. Appl. Phys. Lett., **62** (14), 1585 (1993). DOI: 10.1063/1.109608
[21] G. Brummer, D. Nothern, A.Y. Nikiforov, T.D. Moustakas. Appl. Phys. Lett., **106** (22), 221107 (2015). DOI: 10.1063/1.4922215
[22] H. Morkoç. *Handbook of Nitride Semiconductors and Devices, GaN-Based Optical and Electronic Devices.* (Wiley-VCH, Weinheim: Chichester, 2008), v. 53.
[23] S. Yoshida, K. Ikeyama, T. Yasuda, T. Furuta, T. Takeuchi, M. Iwaya, S. Kamiyama, I. Akasaki. Jpn. J. Appl. Phys., **55** (5S), 05FD10 (2016). DOI: 10.7567/JJAP.55.05FD10
[24] W. Muranaga, T. Akagi, R. Fuwa, S. Yoshida, J. Ogimoto, Y. Akatsuka, S. Iwayama, T. Takeuchi, S. Kamiyama, M. Iwaya, I. Akasaki. Jpn. J. Appl. Phys., **58** (SC), SCCC01 (2019). DOI: 10.7567/1347-4065/ab1253
[25] T. Yasuda, T. Takeuchi, M. Iwaya, S. Kamiyama, I. Akasaki, H. Amano. Appl. Phys. Express, **10** (2), 025502 (2017). DOI: 10.7567/APEX.10.025502
[26] C. Zhang, R. ElAfandy, J. Han. Appl. Sciences, **9** (8), 1593 (2019). DOI: 10.3390/app9081593
[27] J. Chang, D. Chen, L. Yang, Y. Liu, K. Dong, H. Lu, R. Zhang, Y. Zheng. Scientific Reports, **6** (1), 1 (2016). DOI: 10.1038/srep29571.
[28] H. Kogelnik, C.V. Shank. J. Appl. Phys., **43** (5), 2327 (1972). DOI: 10.1063/1.1661499
[29] S.Yu. Karpov, S.N. Stolyarov. Phys. Usp. **36** (1), 1 (1993). DOI: 10.1070/PU1993v036n01ABEH002061
[30] N.N. Martynov, S.N. Stolyarov. Soviet J. Quant. Electron., **8** (8), 1056 (1978). DOI: 10.1070/QE1978v008n08ABEH010615
[31] M. Born, E. Volf. *Osnovy optiki* (Nauka, Gl. red. Fizmatlit, 1973) (in Russian)
[32] J. Dorsaz, J.F. Carlin, S. Gradecak, M. Ilegems. J. Appl. Phys., **97** (8), 084505 (2005). DOI: 10.1063/1.1872197
[33] R. Butté, J.F. Carlin, E. Feltin, M. Gonschorek, S. Nicolay, G. Christmann, D. Simeonov, A. Castiglia, J. Dorsaz, H.J. Buehlmann, S. Christopoulos, G. Baldassarri Höger von Högersthal, A.J.D. Grundy, M. Mosca, C. Pinquier, M.A. Py, F. Demangeot, J. Frandon, P.G. Lagoudakis, J.J. Baumberg, N. Grandjean. J. Phys. D: Appl. Phys., **40** (20), 6328 (2007). DOI: 10.1088/0022-3727/40/20/S16
[34] R. Goldhahn, C. Buchheim, P. Schley, A.T. Winzer, H. Wenzel. *Optical Constants of Bulk Nitrides. In Nitride Semiconductor Devices: Principles and Simulation* (Wiley Weinheim, Germany, 2007)
[35] („Refractive index database“) [Online source]. URL: https://refractiveindex.info (date of application: 01.05.2019).
[36] C.C. Kao, Y.C. Peng, H.H. Yao, J.Y. Tsai, Y.H. Chang, J.T. Chu, H.W. Huang, T.T. Kao, T.C. Lu, H.C. Kuo, S.C. Wang, C.F. Lin. Appl. Phys. Lett., **87** (8), 081105 (2005). DOI: 10.1063/1.2032598
[37] W.Y. Lin, D.S. Wuu, S.C. Huang, R.H. Horng. IEEE Transactions on Electron Devices, **58** (1), 173 (2010). DOI: 10.1109/TED.2010.2084579